

Investigation of Surface Flow Behaviors on Wing Model Made of Different Airfoils

Selim TANGÖZ^{1,a}

¹Erciyes University, Faculty of Aeronautics and Astronautics, Kayseri, Türkiye

^aORCID: 0000-0002-8284-1326

Article Info

Received : 03.07.2024

Accepted : 27.09.2024

DOI: 10.21605/cukurovaumfd.1560184

Corresponding Author

Selim TANGÖZ

stangoz@erciyes.edu.tr

Keywords

Different airfoils

Flow behaviors

Oil visualization

Wing model

How to cite: TANGÖZ, S., (2024). Investigation of Surface Flow Behaviors on Wing Model Made of Different Airfoils. Cukurova University, Journal of the Faculty of Engineering, 39(3), 759-770.

ABSTRACT

This article is focused on the flow behavior observed using the surface oil visualization method on a wing model consisting of four airfoils. In this way, it is aimed to contribute to the insufficient number of literature studies in which flow behaviors are examined by visualization in the wing model consisting of different profiles. The flow behaviors on the surface of the wing and the surface of airfoils forming the wing are presented at three different Reynolds numbers (2×10^5 , 3×10^5 and 4×10^5) and a range of distinct attack angles ranging from 0 to 40 degrees. The tests were applied in a low-speed wind tunnel. After the surface imaging experiments, separation point, reattachment point, and bubble length values reflecting flow behavior were measured for the wing and each airfoil. The flow on surface was trying to transition from laminar to turbulent at angles of attack between 0-16 degrees and the turbulent flow attempted to spread or reattach over the entire surface at between 24-40 degrees. Increasing of the angle of attack and Reynolds number led to reducing the x/c values numerically, weakening the surface separation bubble, and inducing it to shift towards the leading edge. In terms of x/c value, the wing model generally follows a trend close to airfoil B at 0 and 8 degrees and close to airfoil A at 16 degrees. Additionally, the flow behaviors on the wing model are similar to airfoils A and B in terms of the flow phenomena.

Farklı Profillerden Meydana Gelen Kanat Modelinde YüzeY Akış Davranışlarının İncelenmesi

Makale Bilgileri

Geliş : 03.07.2024

Kabul : 27.09.2024

DOI: 10.21605/cukurovaumfd.1560184

Sorumlu Yazar

Selim TANGÖZ

stangoz@erciyes.edu.tr

Anahtar Kelimeler

Kanat modeli

Farklı profiller

Akış davranışları

Yağ görselleştirme

Atf şekli: TANGÖZ, S., (2024). Investigation of Surface Flow Behaviors on Wing Model Made of Different Airfoils. Cukurova University, Journal of the Faculty of Engineering, 39(3), 759-770.

ÖZ

Bu makalede, yüzeY yağ görselleştirme yöntemi kullanılarak dört farklı profilden oluşan bir kanat modeli üzerinde akış davranışları incelenmiştir. Kanadın ve kanadı oluşturan profillerin yüzeYindeki akış davranışları üç farklı Reynolds sayısında (2×10^5 , 3×10^5 ve 4×10^5) ve 0 ile 40 derece arasında değişen farklı hücum açılarında sunulmaktadır. Deneyler düşük hızlı bir rüzgâr tüneline gerçekleştirilmiştir. YüzeY görüntüleme deneylerinden elde edilen ve akış davranışını yansıtan ayrılma noktası, yeniden bağlanma noktası ve kabarcık uzunluğu değerleri sunulmuştur. 0-16 derece arasındaki hücum açılarında yüzeYdeki akış laminerden türbülansa dönüşmeye çalışırken, türbülanslı akış ise 24-40 derece arasındaki hücum açılarında tüm yüzeYe yayılmaya ya da yeniden tutunmaya çalışmaktadır. Hücum açısının veya Reynolds sayısının artması x/c değerlerinde sayısal olarak azalmaya neden olmuş, yüzeY ayrılma balonunu zayıflatmış ve hücum kenarına doğru kaymasına neden olmuştur. X/c değeri açısından kanat modeli genel olarak 0 ve 8 derecede B profiline, 16 derecede ise A profiline yakın bir trend izlemektedir. Ayrıca kanat modelindeki akış davranışları, akış fenomenleri açısından A ve B profillerine benzediği görülmüştür.

1. INTRODUCTION

The flow behavior on the airfoil surface significantly affects the aerodynamic characteristics of the airfoil. The phenomena reflecting flow behavior, as can be seen in Figure 1, have been analyzed and visually presented in diverse studies [1-4].

When studies on flow behavior were examined, it was seen that different flow phenomena occur on the surface, as shown in Figure 1 and Figure 2. As laminar flow transitions to turbulent flow, it was observed that Tollmien-Schlichting waves (T/S waves) first formed in a direction perpendicular to the flow. T/S waves began to form when the Reynolds number of the current reached the indifference Reynolds number [5]. If the amplitude of the primary T/S waves was large enough, the T/S waves moved downstream due to the perturbations of the secondary instabilities.

It lead to a characteristic lambda (λ) structure formation. The λ -vortices were replaced by turbulent points, which initiated the transition to fully turbulent boundary-layer flow [5,6].

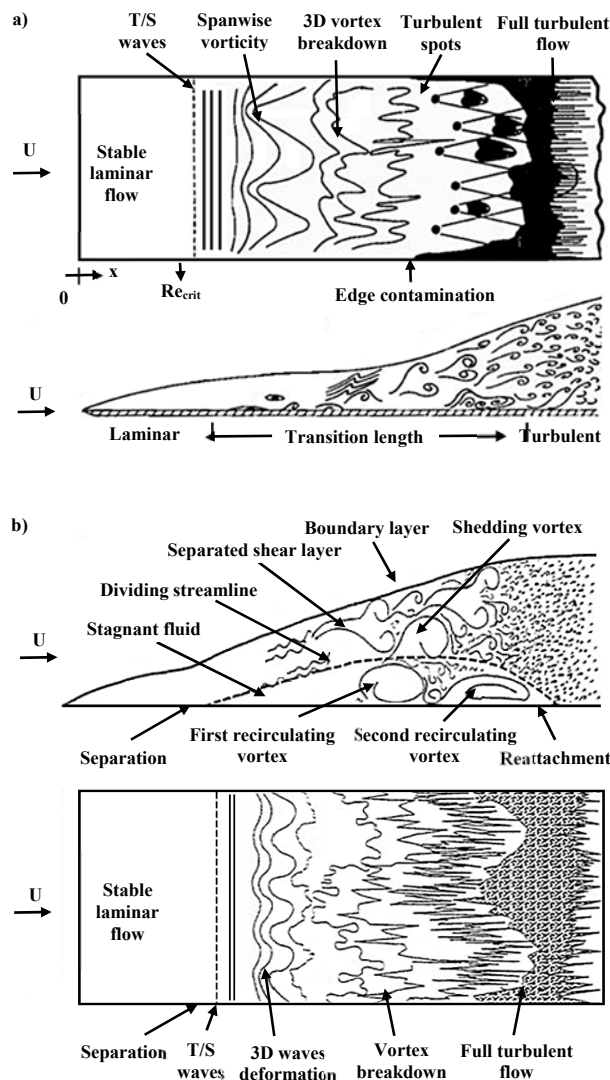


Figure 1. The visualization of flow behavior on surface (a) [1], (b) [2]

Additionally, as seen in Figure 1, a transitional separation bubble could be formed on the surface. Following laminar boundary layer separation, an unstable detached shear layer was created and alteration to turbulence took spot in this shear layer. The boosted momentum transport in the turbulent flow ordinary enabled reconnecting and a turbulent boundary layer developed downstream. After separation, a dead-air region formed under the shear layer. Then, reverse flow and an intense recirculation zone were created near the back of the bubble distribution in the dead-air region [7,8]. Images taken from some studies [9-13] expressing the characteristics of flow behaviors are given in Figure 2.

The surface oil flow visualization method is a simple but effective method that is widely used to follow the flow behavior on the surface of aerodynamic elements. It is quite economical compared to other flow imaging methods. Recently, many studies have been conducted to observe flow behavior using this method. Genç et al. [9] examined the flow behavior on the NACA2415 profile surface at 0.5×10^5 , 1.0×10^5 , and 2.0×10^5 Reynolds numbers and 4, 8, 12, and 15-degree angles of attack. In this context, the separation point, transition point, reattachment point and length of the separation bubble were analyzed using kerosene, titanium dioxide, and a very small amount of oleic acid. At the end of the study, it was observed that when the attack angle increased the separation, transition and reattachment points shifted towards the leading edge and, the length of the separation bubble shortened. In addition, it was determined that as the Reynolds number raised, the transition and reconnect points generally moved towards the leading edge and the bubble length decreased.

In another study, Karthikeyan et al. [10] investigated experimental the effect of the wavy leading ledge of a NACA 4415 profile at Reynolds number of 1.2×10^5 and angles of attack of 6° and 18° . In the study, the separation point, transition point, reattachment point, reverse flow, dead air region and separation bubble were visualized on the surface of the baseline airfoil and the airfoil with tubercles.

In another study examining surface flow behaviors, McGranahan and Selig [11] examined surface flow behavior both experimentally and numerically on nine airfoils at low Reynolds numbers of 2×10^5 , 3.5×10^5 and 5×10^5 . In addition, the aerodynamic performance parameters of the airfoils were analyzed with a numerical computer program. These tests were applied at between -2 and 16 -degree angles. Additionally, fluorescent pigments and fluorescent light were used for flow visualization. Unlike other studies, the parameters such as laminar separation, transition, oil accumulation, reattachment and turbulent separation, which express flow behavior, were presented graphically. As a result of the studies, it was determined that the parameters showing the flow behavior shifted to the leading edge as the angle of attack increased in almost all airfoils. Although the study of McGranahan and Selig [11] is similar to the research presented in this article, the study does not include analyses of any wing models consisting of airfoils. In a similar study, Liu and Hsiao [12] experimentally investigated the aerodynamic properties and flow structures of rectangular wings at aspect ratios varying from 1.0 to 3.0 and Reynolds number between 10^4 and 10^5 . The studies of surface oil flow visualization were illustrated at 10, 20, 30, and 40-degree angles of attack and $Re=1 \times 10^5$. It was observed that the flow separations started in the regions close to the leading edge of the wing and as the angle of attack increased, the separation shifted to the leading edge. In addition, it was indicated at 10° and 20° that the reattachment line was formed in the regions close to the leading edge and just below the separation.

In studies in which wing tip vortices were effective, it was seen that secondary flow occurs with the effect of the wing tip and leading-edge vortices [12]. Additionally, at high angles of attack, the separation bubble and wake flow region appeared to spread over the entire surface [12,13].

Also, it was observed that a secondary flow region, which was formed by the effect of leading-edge separation and wing tip vortices, was shaped at the edges of the reattachment zone. At 30 and 40 degrees, a wake flow region, which was behind the turbulent boundary layer separation line, was formed on most of the surface. Additionally, when the attack angle increases, the region grows and shifts to the leading edge.

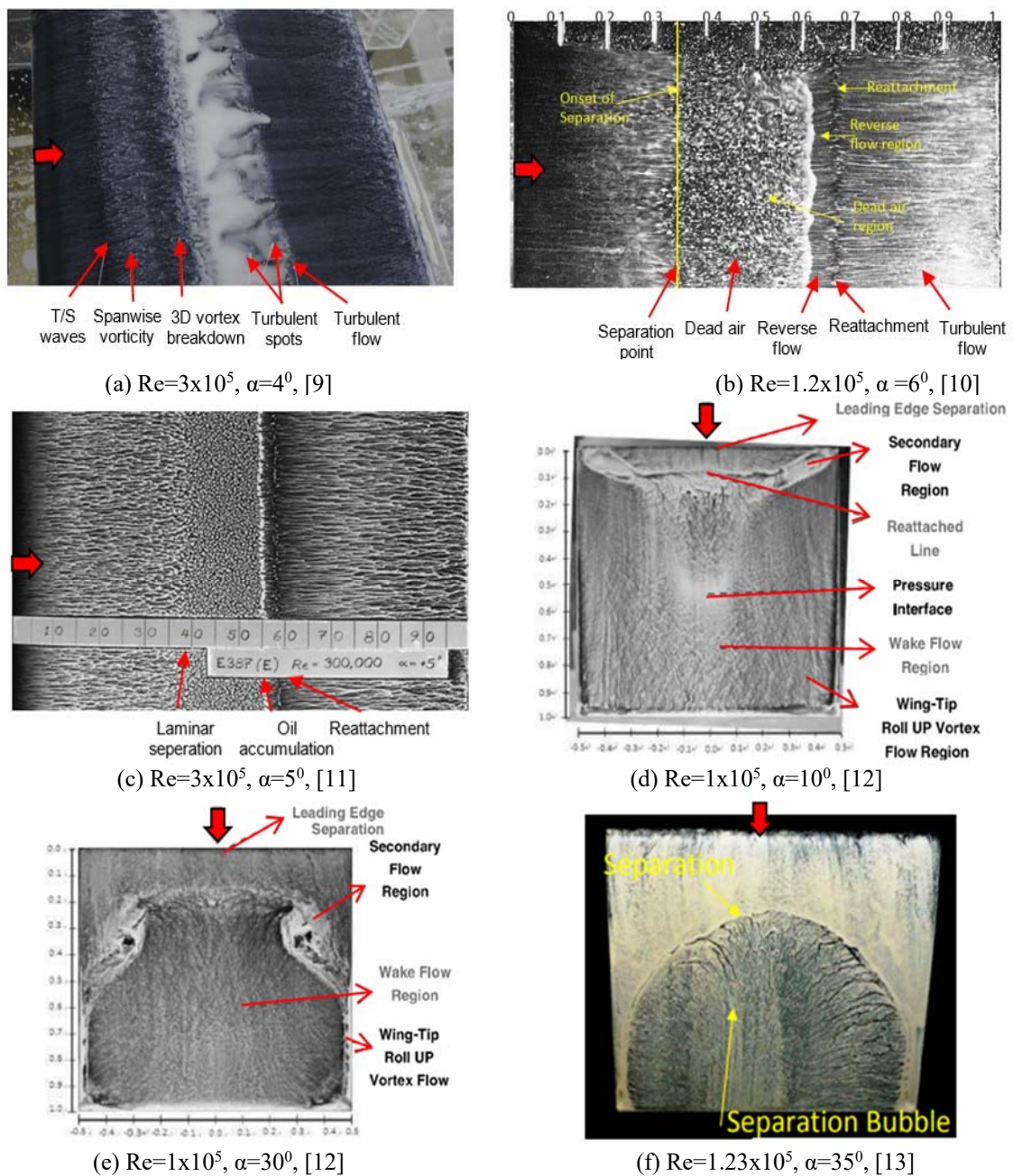


Figure 2. The flow views at different Reynolds numbers and attack angles

The flow behaviors obtained in the study are very similar to the flow behaviors presented in this article. However, NACA 4 and NACA 0012 airfoils with distinct features were used in the study. The wing model obtained from the airfoils was not included in the study. Chen et al. [13] analyzed the flow behavior while examining the effect of protuberances on the leading edge of a wing model on aerodynamic performance. The studies were carried out at a constant flow rate and constant Reynolds number at distinct angles of attack between 13 and 40 degrees and at aspect ratios of 1, 2, and 3. In this study, separation bubbles, separation zones, reattachment points and similar flow behaviors were presented by visualizing using a composite solution forming of kerosene, titanium dioxide and oleic acid by a mass ratio of 6:3:2.

When the figures in the article are examined, it is clearly seen that while laminar and turbulent flows occur on the wing surface at low angles of attack, the turbulent zone spreads over the entire surface at high angles of attack. Although this study is similar to the existing study presented in the article because it is carried out at low and high angles of attack, the main difference is that the wing model consists of a single airfoil. Wang et al. [14] observed the flow behavior while examining the effects of blowing and suction methods on the wind turbine airfoil on the NACA 0012 airfoil in a low-speed wind tunnel. In the study conducted at 14-degree angle of attack and 1.0×10^5 Reynolds number, separation points, separation bubbles and reattachment behaviors were inspected using a mix was made of titanium dioxide, silicon oil, dodecane and oleic acid. Trie et al. [15] researched the behavior of flow on NACA 43018 airfoil with a parabolic vortex generator at 1.0×10^5 and 2.0×10^5 Reynolds numbers and 0, 4, 10, 12, 15 and 17-degree angles of attack. In this experimental research, the points of separation, transition and reattachment, spanwise vorticity, turbulent/laminar flow, T/S waves and 3d vortex breakdown showed the flow behavior on the airfoil surface was investigated.

Many flow visualization studies [16-24] similar to the studies whose summary given above have been carried out. However, most visualization studies have been conducted on a single airfoil. In this article, the flow behaviors have been analyzed on the wing model obtained from four airfoils. For this reason, the present study differs from other literature studies.

2. EXPERIMENTAL ARRANGEMENT AND PROCEDURES

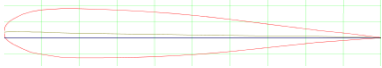

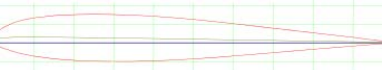

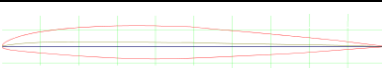

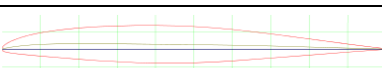

The flow visualization research presented in the paper was tested out in a low-speed tunnel in the Aerodynamics Research Laboratory at Erciyes University Faculty of Aeronautics and Astronautics. The wind tunnel's test section has a 57×57 cm quadratic inlet and 59×59 cm quadratic outlet of 180 cm length. Other details of the wind tunnel can be found in [25]. A view of the tunnel is shown in Figure 3. For the flow analysis, profiles forming the wing of a commercially used aircraft were selected in the experimental study. Profiles forming the inner, middle and outer wings of the wing were used. The airfoils and the wing model used in surface flow visualization have been produced from grey polylactic acid thermoplastic polyester with the help of a 3D printer. The airfoils and the wing model have a 21cm cord length and 1.0 aspect ratio. The model wing is composed of four airfoils [25]. The features of the airfoils and the wing model and the location of the airfoils on the wing model are given in Table 1.

The flow visualization experiments were carried out at 0, 4, 8, 12, 16, 20, 24, 32 and 40-degree angles of attacks and 2×10^5 , 3×10^5 and 4×10^5 Reynolds numbers, respectively. To ensure the flow regime, flow images were recorded after the wind tunnel was operated for 3-5 minutes, depending on the flow rate. Additionally, each study was repeated at least twice, at several times, to ensure the correct flow regime was established. Silica oil, oleic acid and titanium dioxide mixtures, which are widely used in the literature, were used for flow visualization. As a result of the experiments which were conducted with different mixing ratios and different viscosity silicone oils, it was found suitable to have a mixture of silicone oil, oleic acid and titanium dioxide in the ratio of 8:1:1, with silicone oil with a viscosity of 5 cSt for the best visualization. The images of airfoil D applied the mixture to the surface when the wind tunnel was closed and of the measuring device used to gauge the flow points are given in Figure 3.



Figure 3. Views of the wind tunnel [25] and of the oil mixture on airfoil D surface

Table 1. The airfoil forms, characteristics and locations in the model wing of the airfoil. [25,26].

Airfoil	Forms of airfoil	Maximum thickness/ location (% of chord)	Maximum camber/ location (% of chord)	Location on model wing (% of span)	Views of airfoils on model wing
b737a (Airfoil A)		15.4 / 19.6	0.2 / 5	0	
b737b (Airfoil B)		12.5 / 29.7	0.8 / 10	33.3	
b737c (Airfoil C)		10 / 39.9	1.5 / 20.4	66.6	
b737d (Airfoil D)		10.8 / 40	1.6 / 20	100	

3. RESULTS AND DISCUSSIONS

In the section, the flow behaviors on the surface of the wing model and airfoils are analyzed in terms of visually and dimensionally at 2×10^5 , 3×10^5 and 4×10^5 Reynolds numbers and different attack angles range from 0 to 40 degrees.

The images obtained in the studies can be divided into two groups in terms of visuals. 1. In studies between 0-16 degrees, the flow on the surface is trying to transition from laminar flow to turbulent flow. In there, although there are differences in location and size/length, it is seen that the flow generally exhibits similar behavior during the transition from laminar flow to turbulent flow on surfaces where wing tip vortices are inactive. 2. In studies between 24-40 degrees, the turbulent flow is trying to spread or reattach over the entire surface. The flow behaviors observed are compatible with literature studies [9-12,22,26-28] tested out at different angles of attack from 0 degrees to 40 degrees.

Figure 4 shows the oil flow image on the wing model surface under the influence of wing tip vortices at 8 degrees and 3×10^5 Reynolds number.

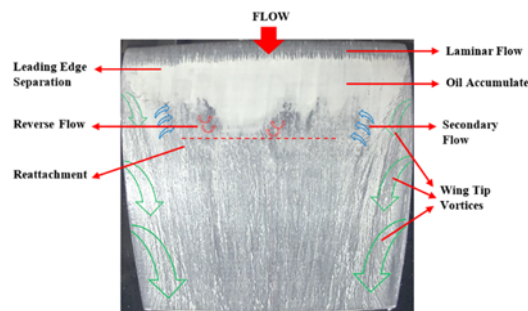


Figure 4. Flow properties on the surface of the wing model at $\alpha=8^\circ$ and $Re=3 \times 10^5$.

In the figure, the laminar flow begins to separate in the regions close to the leading edge and then continues its flow by re-attachment itself in the middle regions where the wing tip vortices do not have any effect. Also, it is observed that the flow in the regions close to the wing tip shifts towards the inner parts as it moves from the leading edge to the trailing edge (as expected). Moreover, the secondary flow formed by the effect of the wing tip vortices and reverse flow forces the oil flow to accumulate in the middle regions of the surface.

The oil flow image on the wing model surface under the influence of wing tip vortices at 24 degrees and 3×10^5 Reynolds number is indicated in Figure 5. Due to the high angle of attack, the flow separation starts at very close points to the leading edge. Wing tip vortexes are quite strong in the middle parts of the wing. However, it does not occur at all in regions close to the trailing edge due to the effect of turbulent flow. Secondary flow occurs at both ends of the wing and at points close to the leading edge because of the wing

tip vortices effect. Moreover, it can be seen that the current is trying to reattachment weakly, in regions close to the leading edge and where is not affected by the wing tip vortex.

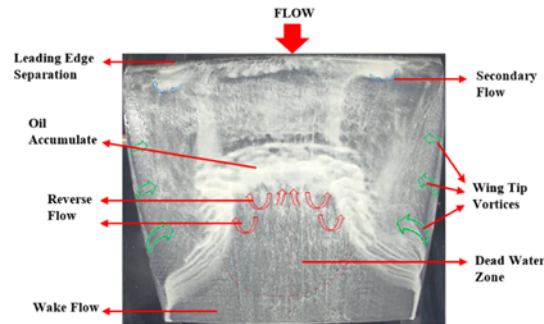


Figure 5. Flow properties on the surface of the wing model at $\alpha=24^\circ$ and $Re=3 \times 10^5$.

Due to the effect of the large separation bubble formed in the regions close to the trailing edge, reverse flow emerges towards the leading edge, and this reverse flow causes the oil to accumulate in the form of a dome in the middle region. A dead flow zone, which is the flow partially stops, begins just below the reverse flow as approaches to the trailing edge. It is seen that wake flow emerges only in the regions close to the trailing edge, owing to the large separation bubble effect.

In the section, the flow behaviors are analyzed in terms of dimensionally such as separation point, reattachment point and bubble length at different Reynolds numbers and attack angles ranging from 0 to 40 degrees.

Table 2-4 and Figure 6-10 represent dimensionally the separation point, reattachment point and bubble length that emerged from flow views. Additionally, Table 5 gives the views of flow at 3×10^5 Reynolds number and 0° , 8° , 16° , 24° , 32° and 40° attack angles for the airfoils and the wing model. While creating the numerical values, the methods present in some literature studies [28-31] have been used.

Table 2. Separation point (C_s), reattachment point (C_r) and bubble length (L_b) for airfoil A

Re	α [$^\circ$]	C_s [x/c]	C_r [x/c]	L_b [x/c]
2×10^5	0	0.075	0.3	0.225
	8	0.05	0.25	0.2
	16	0.05	0.2	0.15
3×10^5	0	0.085	0.275	0.19
	8	0.05	0.215	0.165
	16	0.05	0.175	0.125
4×10^5	0	0.1	0.275	0.175
	8	0.05	0.2	0.15
	16	0.025	0.125	0.1

The separation point, reattachment point and bubble length for airfoil A are offered in Table 2. While the angle of attack increases at a constant Reynolds number, the C_s , C_r and L_b values decrease. In other words, an increase in the angle of attack pulls the laminar separation and reattachment on the surface towards the leading edge and weakens the separation bubble.

At 3×10^5 Reynolds number, as the angle of attack is increased from 0 degrees to 16 degrees, the C_s value decreases from 0.085 to 0.05, the C_r value declines from 0.275 to 0.175 and the L_b value drops from 0.19 to 0.125.

At a constant angle of attack, increasing the Reynolds number reduces the C_r and L_b values, but does not have a significant effect on the C_s values. Increasing the Reynolds number pulls the reattachment towards the leading edge and weakens the separation bubble. For example, at 8 degrees for airfoil A, while the Reynolds number is increased from 2×10^5 to 4×10^5 , the C_s value remains constant at 0.05, the C_r and L_b have values of 0.25, 0.215, 0.2, and 0.2, 0.165, 0.15, respectively.

Figure 6 displays numerical values (x/c) of separation point, reattachment point and bubble length for airfoil B. When the changes in the figures are checked, it is seen that C_s values are 0.05, 0.025, and 0, C_r values are 0.675, 0.3, and 0.0175 and L_b values are 0.625, 0.275 and 0.0175 at 0, 8 and 16 degrees for 2×10^5 Reynolds number. When the Reynolds number is 3×10^5 , C_s is obtained as 0.15, 0.05 and 0 at 0, 8 and 16 degrees. C_r value is obtained as 0.575, 0.225, 0.1, and L_b is obtained as 0.425, 0.175 and 0.1 at the same degrees, respectively. While the Reynolds number is 4×10^5 , at 0, 8, and 16 degrees C_s are 0.15, 0.05, 0, C_r are 0.5, 0.2, 0.1 and L_b are 0.35, 0.15, 0.1, respectively.

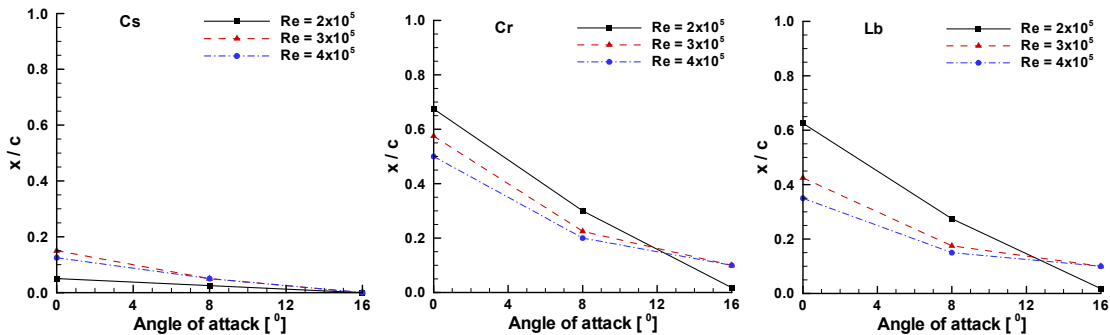


Figure 6. x/c values of C_s , C_r and L_b for airfoil B versus angle of attack

When the figures and numerical values in Table 2-4 and Figure 6-10 are examined, two important effects can be seen. Increasing the angle of attack or Reynolds number numerically reduces the values that determine the boundaries of the separation bubble and weakens the surface separation bubble, causing it to shift towards the leading edge.

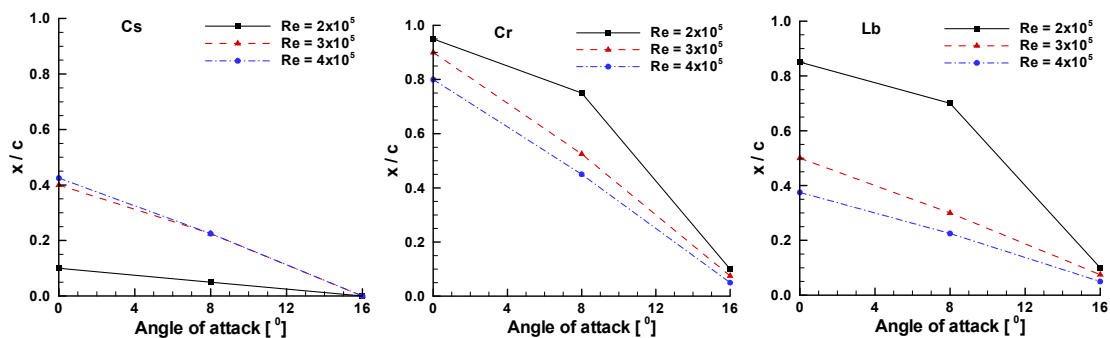


Figure 7. x/c values of C_s , C_r and L_b for airfoil D versus angle of attack

When Table 5 is examined, it is seen that there are similar changes in the x/c values of C_s , C_r , and L_b at three different Reynolds numbers. As each C_s , C_r , and L_b changes are checked, it is viewed that x/c data is higher in airfoils C and D having lower thickness but higher camber at angles of attack of 0 and 8 degrees.

Table 3. Separation point (C_s), reattachment point (C_r) and bubble length (L_b) for airfoil C

Re	α [$^\circ$]	C_s [x/c]	C_r [x/c]	L_b [x/c]
2×10^5	0	0.1	0.95	0.85
	8	0.05	0.75	0.7
	16	0	0.06	0.06
3×10^5	0	0.25	0.875	0.625
	8	0.11	0.45	0.34
	16	0	0.04	0.04
4×10^5	0	0.35	0.8	0.45
	8	0.1	0.275	0.175
	16	0	0.025	0.025

At the same angle, the x/c value is lower in airfoils A and B which have high thickness but low camber. At these angles, it can be said that the x/c value is inversely proportional to the thickness and directly proportional to the camber. Moreover, it is observed that the situation is reversed at 16 degrees. Relevant x/c values are higher in airfoils with greater thickness and low camber.

Although these values remain in the middle in the wing model consisting of airfoils, it is sighted that it generally follows a trend close to airfoil B up to 8 degrees and close to airfoil A after 8 degrees. To summarize, at low angles of attack, in thick and low-camber profiles and partially in the wing model, laminar separation, reattachment and the separation bubble occur in regions closer to the leading edge and the length of the bubble becomes shorter. At a high angle of attack, a similar situation occurs for thin and more camber profiles. Although different results were obtained in the studies [30,32,33], it was generally determined that the separation bubble shortened and shifted towards

the leading edge as the thickness and camber increased. When the results obtained in the current study are examined, it is evaluated that the thickness is effective on the size and location of the separation bubble at low angles of attack (0 and 8 degrees), while the camber is more effective at 16 degrees.

Table 4. Separation point (Cs), reattachment point (Cr) and bubble length (Lb) for the wing model

Re	α [°]	Cs [x/c]	Cr [x/c]	Lb [x/c]
2x10 ⁵	0	0.05	0.775	0.725
	8	0.05	0.3	0.25
	16	0.025	0.2	0.175
3x10 ⁵	0	0.1	0.625	0.525
	8	0.025	0.225	0.2
	16	0	0.125	0.125
4x10 ⁵	0	0.35	0.62	0.27
	8	0.05	0.225	0.175
	16	0	0.1	0.1

When the flow images at 24 and 32 degrees are examined, phenomena such as reverse flow, secondary flow and wing tip vortices are seen. Additionally, as the Reynolds number increases, it is generally observed that the separation bubble spreads more on the surface and partially slides towards the leading edge.

The flow behaviors on the wing model are similar to the flow behaviors of airfoils A and B in terms of the flow phenomena. When the images at 40 degrees are examined, it is seen that the flow completely breaks away from the surface in all profiles at 2x10⁵ Reynolds number. It is seen that at Reynolds numbers 3x10⁵ and 4x10⁵, the flow can reattach to the surface in regions close to the trailing edge. As the Reynolds number increases, the reattachment point of the current shifts toward the leading edge.

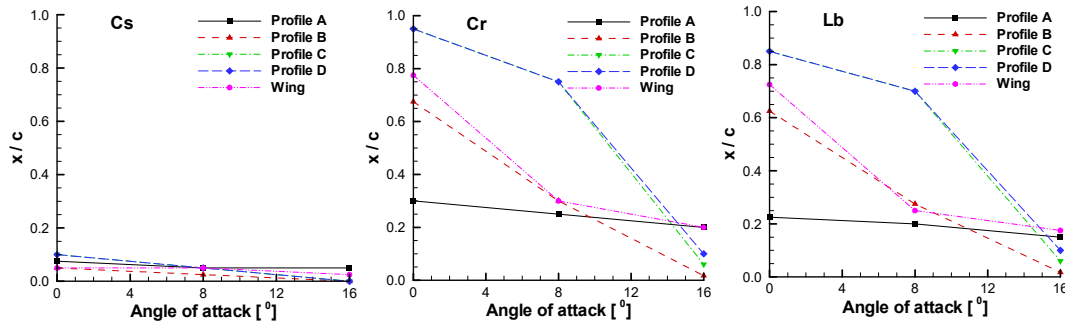


Figure 8. x/c of Cs, Cr and Lb for the airfoils and the wing model versus attack angle at 2x10⁵ Reynolds number

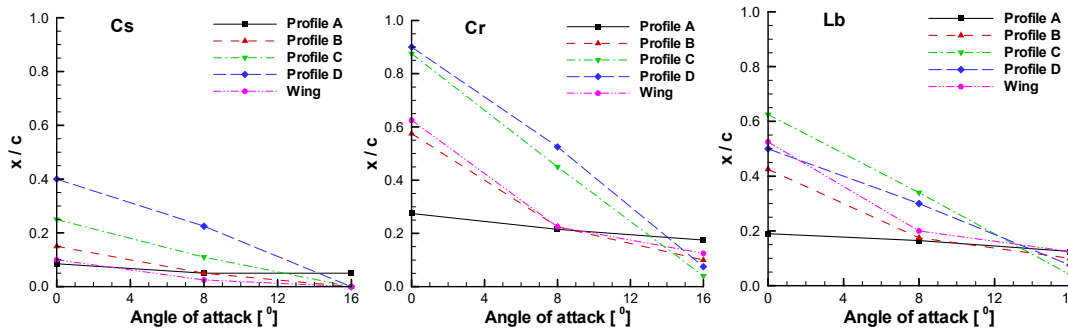


Figure 9. x/c values of Cs, Cr and Lb for the airfoils and the wing model versus attack angle at 3x10⁵ Reynolds number

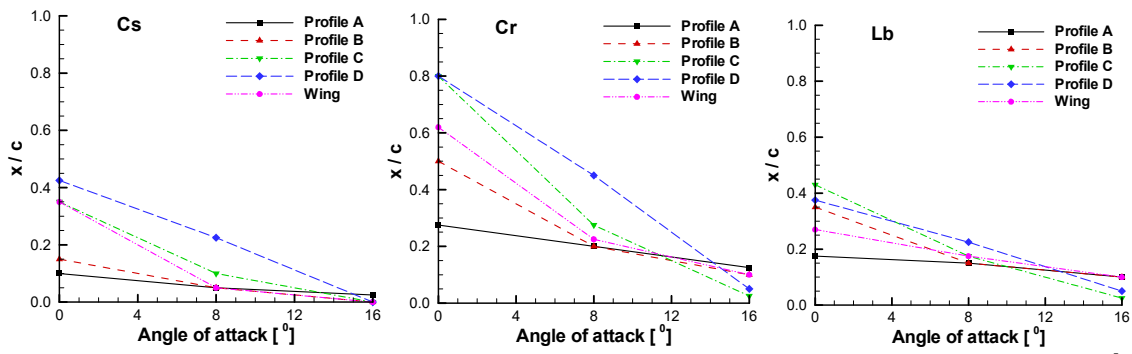


Figure 10. x/c values of C_s , C_r and L_b for the airfoils and the wing model versus attack angle at 4×10^5 Reynolds number

Table 5. Flow views on the surface of airfoils and wing model at $Re = 3 \times 10^5$.

	Airfoil-A	Airfoil -B	Airfoil -C	Airfoil -D	Wing model
$\alpha = 0^\circ$					
$\alpha = 8^\circ$					
$\alpha = 16^\circ$					
$\alpha = 24^\circ$					
$\alpha = 32^\circ$					
$\alpha = 40^\circ$					

4. CONCLUSIONS

The flow behaviors on the surfaces of the wing model and of the four airfoils forming the wing model are analyzed visually and dimensionally at different Reynolds numbers and angles of attack. The following results are obtained from the experiments.

- The flow on the surface is trying to transition from laminar to turbulent at angles of attack of 0, 8, and 16 degrees.
- The turbulent flow is trying to spread or reattach over the entire surface at between 24-40 degrees.
- At a fixed angle of attack, the increase in Reynolds number increases the kinetic energy of the flow, thus pulling the reattachment towards the leading edge and weakening the separation bubble.
- The increase in Reynolds number improves the kinetic energy of the flow over the wing and for this reason it numerically reduces the x/c values for C_r , C_s , and L_b of the separation bubble.
- While the x/c value is higher in airfoils C and D having higher camber at angles of attack of 0 and 8 degrees, the x/c value is lower in airfoils A and B having high thickness. At 16 degrees, the situation turns into reverse, so the x/c value is higher in airfoils A and B. The x/c values remain in the middle of the wing model. The wing model generally follows a trend close to airfoil B at 0 and 8 degrees and close to airfoil A at 16 degrees. At low angles of attack between 0-8°, increasing the camber, which increases the lift force, delays the formation of bubbles in the more cambered C and D airfoils. At around 16°, an increase in the thickness, which increases the lift and stall angle, delays the formation of bubbles in the more thickness A and B airfoils.

5. ACKNOWLEDGEMENT

Thanks to the Unit of the Scientific Research Projects of Erciyes University (FBA-2018-7827) and Dr. Abdulhalim Aşkan for their past contributions in the production of the profiles. Additionally, I would like to thank the Proofreading & Editing Office of the Dean for Research at Erciyes University for copyediting and proofreading service for this manuscript.

6. REFERENCES

1. White, F.M., 1991. Viscous fluid flow. Second Edition, McGraw-Hill Inc., New York, 376.
2. LaGraff, J.E., Ashpis, D.E., 1998. Minnowbrook II 1997 workshop on boundary layer transition in turbomachines. National Aeronautics and Space Administration, NASA/CP-1998-206958, 345.
3. Versteeg, H.K., Malalasekera, W., 1995. An introduction to computational fluid dynamics the finite volume method. Longman Scientific and Technical, 47.
4. Cherubini, S., Picella, F., Robinet, J.C., 2021. Variational nonlinear optimization in fluid dynamics: the case of a channel flow with superhydrophobic walls. *Mathematics*, 9(53), 1-25.
5. Schlichting, H., Gersten, K., 2017. Boundary-layer theory. Ninth Edition, Springer-Verlag Berlin Heidelberg, 419-420.
6. Bowles, R.I., 2000. Transition to turbulent flow in aerodynamics. *Philosophical Transactions: Mathematical, Physical and Engineering Sciences*, 358(1765), 245-260.
7. Horton, H.P., 1968. Laminar separation bubbles in two and three-dimensional incompressible flow. PhD Thesis, University of London, 28-30.
8. Sandham, N.D., 2008. Transitional separation bubbles and unsteady aspects of airfoil stall. *The Aeronautical Journal*, 112(1133), 395-404.
9. Genç, M.S., Karasu, İ., Açıkel, H.H., 2012. An experimental study on aerodynamics of NACA2415 airfoil at low Re numbers. *Experimental Thermal and Fluid Science*, 39, 252-264.
10. Karthikeyan, N., Sudhakar, S., Suriyanarayanan, P., 2014. Experimental studies on the effect of leading-edge tubercles on laminar separation bubble. AIAA 2014-1279. 52nd Aerospace Sciences Meeting, 1-9.
11. McGranahan, B.D., Selig, M.S., 2003. Surface oil flow measurements on several airfoils at low Reynolds numbers. 21st AIAA Applied Aerodynamics Conference, AIAA 2003-4067, 1-18.
12. Liu, Y.C., Hsiao, F.B., 2014. Experimental investigation on critical Reynolds numbers aerodynamic properties of low aspect ratios wings. *Procedia Engineering*, 79, 76-85.
13. Chen, J.H., Li, S.S., Nguyen, V.T., 2012. The effect of leading-edge protuberances on the performance of small aspect ratio foils. 15th International Symposium on Flow Visualization.

14. Wang, L., Alam, M.M., Rehman, S., Zhou, Y., 2022. Effects of blowing and suction jets on the aerodynamic performance of wind turbine airfoil. *Renewable Energy*, 196, 52-64.
15. Trie, D.Z., Hariyadi, S., Rifdian, I.S., 2023. Experimental study of fluid flow characteristics in wing airfoil NACA 43018 with parabolic vortex generator using oil flow visualization. *Proceedings of the International Conference on Advance Transportation, Engineering, and Applied-Science (ICATEAS 2022)*, 52-69.
16. Kumar, V., Mandal, A.C., Podda, K., 2024. An experimental investigation on the aerodynamic characteristics and vortex dynamics of a flying wing. *The Aeronautical Journal*, First view, 1-25.
17. Mizoguchi, M., Kajikawa, Y., Itoh, H., 2016. Aerodynamic characteristics of low-aspect-ratio wings with various aspect ratios in low Reynolds number flows. *Transactions of The Japan Society for Aeronautical and Space Sciences*, 59, 2, 56-63.
18. Ananda, G.K., Sukumar, Selig, M.S., 2015. Measured aerodynamic characteristics of wings at low Reynolds numbers, *Aerospace Science and Technology*, 42, 392-406.
19. Li, Q., Kamada, Y., Maeda, T., Murata, J., Nishida, Y., 2016. Visualization of the flow field and aerodynamic force on a horizontal axis wind turbine in turbulent inflows. *Energy*, 111, 57-67.
20. Seyhan, M., Akbıyık, H., Sarioğlu, M., Keçecioglu, S.C., 2022. The effect of leading-edge tubercle on a tapered swept-back sd7032 airfoil at a low Reynolds number. *Ocean Engineering*, 266(2), 112794, 1-13.
21. Ghorbanishohrat, F., Johnson, D.A., 2018. Evaluating airfoil behavior such as laminar separation bubbles with visualization and IR thermography methods. *Journal of Physics: Conference Series* 1037, 052037, 1-10.
22. Wei, Z.J., Qiao, W.Y., Liu, J., Duan, W., 2016. Reduction of endwall secondary flow losses with leading-edge fillet in a highly loaded low-pressure turbine. *Proceedings of the Institution of Mechanical Engineers Part a Journal of Power and Energy*, 230(2), 184-195.
23. Genç, M.S., Özhan, G., Özden, M., Kiriş, M.S., Yıldız, R., 2018. Interaction of tip vortex and laminar separation bubble over wings with different aspect ratios under low Reynolds numbers. *Proceedings of the Institution of Mechanical Engineers, Part C: Journal of Mechanical Engineering Science*, 232(22), 4019-4037.
24. Aşkan, A., Tangöz, S., Konar, M., 2023. An investigation of aerodynamic behaviors and aerodynamic performance of a model wing formed from different profiles. *The Aeronautical Journal*, 127(1310), 676-697.
25. Aşkan, A., Tangöz, S., 2018. The impact of aspect ratio on aerodynamic performance and flow separation behavior of a model wing composed from different profiles. *Journal of Energy Systems*, 4(2), 224-237.
26. Duan, W., Qiao, W., Wei, Z., Liu, J., Cheng, H., 2018. The influence of different endwall contouring locations on the secondary flow losses in a highly loaded low-pressure turbine. *Proceedings of the ASME Turbo Expo 2018: Turbomachinery Technical Conference and Exposition, Volume 2B: Turbomachinery*, V02BT41A018 ASME, 1-11.
27. Sudhakar, S., Karthikeyan, N., Suriyanarayanan, P., 2019. Experimental studies on the effect of leading-edge tubercles on laminar separation bubble. *AIAA Journal*, 57(12), 5197-5207.
28. Torres, G.E., Mueller, T.J., 2004. Aerodynamic impact of aspect ratio at low Reynolds number. *AIAA Journal*, 42(5), 865-873.
29. Marchman, J.F., 1987. Aerodynamic testing at low Reynolds numbers. *Journal Aircraft*, 24(2), 107-114.
30. Elgammi, M., Sant, T., Ateeah, A.A., 2022. The influence of the flow separation bubble and transition location on the profile drag of three 4-digit NACA airfoil profiles. *Wind Engineering*, 46(3), 796-817.
31. Traub, L.W., Cooper, E., 2008. Experimental investigation of pressure measurement and airfoil characteristics at low Reynolds numbers. *Journal of Aircraft*, 45(4), 1322-1333.
32. Karasu, İ., Açikel, H.H., Koca, K., Genç, M.S., 2020. Effects of thickness and camber ratio on flow characteristics over airfoils. *Journal of Thermal Engineering*, 6(3), 242-252.
33. Dongli, M., Yanping, Z., Yuhang, Q., Guanxiong, L., 2015. Effects of relative thickness on aerodynamic characteristics of airfoil at a low Reynolds number. *Chinese Journal of Aeronautics*, 28(4), 1003-1015.

NOMENCLATURE

x/c	: Location along the chord	Re	: Reynolds number
α	: Angle of attack	Cs	: Separation point
Cr	: Reattachment point	Lb	: Length of bubble